Eur Biophys J (2011) 40:447–462
DOI 10.1007/s00249-010-0657-0

ORIGINAL PAPER

A kinked antimicrobial peptide from *Bombina maxima*. I. Three-dimensional structure determined by NMR in membrane-mimicking environments

Orsolya Toke · Zoltán Bánóczi · Péter Király · Ralf Heinzmann · Jochen Bürck · Anne S. Ulrich · Ferenc Hudecz

Received: 12 October 2010 / Revised: 9 December 2010 / Accepted: 13 December 2010 / Published online: 14 January 2011

Abstract Maximin-4 is a 27-residue cationic antimicrobial peptide exhibiting selectivity for bacterial cells. As part of the innate defense system in the Chinese red-belly toad, its mode of action is thought to be ion channel or pore formation and dissipation of the electrochemical gradient across the pathogenic cell membrane. Here we present the high-resolution structure of maximin-4 in two different membrane mimetics, sodium dodecyl sulfate micelles and 50% methanol, as determined by ^{1}H solution NMR spectroscopy. In both environments, the peptide chain adopts a helix–break–helix conformation following a highly disordered N-terminal segment. Despite the similarities in the overall topology of the two structures, major differences are observed in terms of the interactions stabilizing the kink region and the arrangement of the four lysine residues. This has a marked influence on the shape and charge distribution of the molecule and may have implications for the bacterial selectivity of the peptide. The solution NMR results are complemented by CD spectroscopy and solid-state NMR experiments in lipid bilayers, both confirming the predominantly helical conformation of the peptide. As a first step in elucidating the membrane interactions of maximin-4, our study contributes to a better understanding of the mode of action of antimicrobial peptides and the factors governing their selectivity.

Keywords Membrane peptides · Lipid bilayers · NMR spectroscopy · Peptide conformation · Bacterial resistance · Maximin

Membrane-active peptides: 455th WE-Heraeus-Seminar and AMP 2010 Workshop.

Electronic supplementary material The online version of this article (doi:10.1007/s00249-010-0657-0) contains supplementary material, which is available to authorized users.

O. Toke (✉) · P. Király
Institute of Structural Chemistry,
Chemical Research Center of the Hungarian Academy of Sciences, 59-67 Pusztaszeri út, 1025 Budapest, Hungary
e-mail: toke@chemres.hu

Z. Bánóczi · F. Hudecz
Research Group of Peptide Chemistry,
Eötvös Loránd University, Hungarian Academy of Sciences,
P.O. Box 32, 1518 Budapest 112, Hungary

R. Heinzmann · J. Bürck · A. S. Ulrich
Karlsruhe Institute of Technology,
Institute for Biological Interfaces (IBG-2),
Institute of Organic Chemistry, Karlsruhe, Germany

F. Hudecz
Department of Organic Chemistry, Eötvös Loránd University,
P.O. Box 32, 1518 Budapest 112, Hungary

Abbreviations

AMP	Antimicrobial peptide
MBHA	4-Methylbenzhydrylamine
DMF	Dimethylformamide
DCM	Dichloromethane
DCC	*N*,*N*′-dicyclohexylcarbodiimide
HOBt	1-Hidroxybenzotriazole
TFA	Trifluoroacetic acid
EDTA	Ethylenediamine tetraacetic acid
PIPES	Piperazine-*N*-*N*′-bis(2-ethanesulfonic acid)
SDS	Sodium dodecyl sulfate
DPC	Dodecylphosphocholine
DPPC	Dipalmitoylphosphatidylcholine
DPPG	Dipalmytoylphosphatidylglycerol
DMPC	Dimyristoylphosphatidylcholine
DMPG	Dimyristoylphosphatidylglycerol
MLV	Multilamellar vesicle

HPLC	High-pressure liquid chromatography
NMR	Nuclear magnetic resonance
TOCSY	Total correlation spectroscopy
NOESY	Nuclear Overhauser effect spectroscopy
HSQC	Heteronuclear single quantum correlation
ARIA	Ambiguous restraints for iterative assignment
RMSD	Root mean square deviation
MAS	Magic-angle spinning
REDOR	Rotational-echo double resonance
CD	Circular dichroism

Introduction

The extensive use of antibiotics over the past few decades (English and Gaur 2010) and the sophisticated genetic and biochemical ways employed by pathogenic bacteria to combat antimicrobial agents (Walsh 2000) have given rise to resistant bacterial strains. The growing threat of microbial resistance has prompted an interest in (1) revitalizing new antibiotics and (2) finding new target sites and drugs. The most promising strategies include genetic or chemoenzymatic alteration of antibiotic-producing modular enzymes (Sieber and Marahiel 2005), modification of carbohydrate moieties in glycopeptide antibiotics (Ge et al. 1999; Lin and Walsh 2004), inhibition of resistance mechanisms (Drawz and Bonomo 2010; Kaatz 2005), and looking for compounds with alternative, nonenzymatic antibiotic modes of action. One such family of substances are the antimicrobial peptides (AMPs), a group of typically short, 10–40-residue polypeptide chains, which as part of the innate defense system provide protection against microorganisms in both vertebrates and invertebrates (Nicolas and Mor 1995; Andreu and Rivas 1998; Tossi et al. 2000; van't Hof et al. 2001; Hancock and Diamond 2000; Boman 2003; Toke 2005). Although in some cases there are indications of the existence of intracellular targets (Ulvatne et al. 2004; Park et al. 1998), the predominant killing mechanism of most AMPs appears to be permeabilization of the cytoplasmic membrane (Matsuzaki 1999; Shai 2002). While some antimicrobial peptides are also toxic to eukaryotic cells, a good portion of them show no hemolytic effect at their antimicrobial concentration. The physical nature of their mode of action in combination with the frequently observed selectivity makes them promising candidates for novel antibiotics (Andres and Dimarcq 2005).

Among the nearly 1,000 AMPs reported so far, peptides of different size, charge, hydrophobicity, and conformation can be found. However, there are certain common features that seem to dominate; for instance, all AMPs have amphipathic character and at physiological pH usually possess net positive charge [although there are a few exceptions to this (Lai et al. 2002a, b; Harris et al. 2009)]. The positive charge helps the peptides to reach their anionic cellular target (Hancock 1997; da Silva and Teschke 2003) and enhances bacterial selectivity, while the spatial segregation between hydrophilic and hydrophobic side-chains determines the binding affinity to lipid bilayers (Dathe and Wieprecht 1999). Amphipathicity and the relative size of the hydrophilic versus hydrophobic face of AMPs are also known to affect the curvature strain exerted by the peptide chains on lipid bilayers (Epand et al. 1995; Wieprecht et al. 1997), thereby influencing the mechanism of pore formation.

Maximin-4 is a 27-residue antimicrobial peptide from the skin secretions of the Chinese red-belly toad *Bombina maxima* with a broad spectrum of antibacterial activity and low hemolytic effect toward red blood cells (Lai et al. 2002a, b). Similarly to other AMPs, its mode of action is thought to be ion channel or pore formation in the bacterial cell membrane. In addition to its antibacterial activity, it has also been found to possess significant cytotoxicity on certain tumor cell lines and some antiviral activity as well. As other maximin peptides, it shows sequence homology with bombinin-like AMPs, particularly with BLP-1 (Gibson et al. 1991) and BLP-2 (Simmaco et al. 1991). Its characteristic physicochemical parameters in comparison with other well-studied AMPs are listed in Table 1.

To obtain a detailed molecular view of the interaction of maximin-4 with membrane systems, we have characterized its structure and orientation in various model membranes using a combination of liquid-state and solid-state NMR methodologies. The present paper is focused on the three-dimensional structure of maximin-4 in SDS micelles and in phospholipid bilayers. For comparison, the NMR structure of the peptide in 50% methanol is also discussed. The accompanying paper by Heinzmann et al. (2010) addresses the molecular alignment of maximin-4 in membrane systems under different conditions.

Materials and methods

Materials

Phospholipids were obtained from Avanti Polar Lipids (Alabaster, AL). Isotopically labeled di-*tert*-butyl dicarbonate amino acids, d_{25}-SDS, d_{38}-DPC, and CD_3OH were from Cambridge Isotope Laboratories (Andover, MA). Natural abundance amino acid derivatives were purchased from Novabiochem (Laufelfingen Switzerland) or Reanal

Table 1 Sequence, origin, hydrophobic moment (μ), charge (z), and hydrophobicity (H) of a few selected antimicrobial peptides

Peptide	Sequence	Origin	μ^a	z^b	H^c
Bombolitin I	IKITTMLAKLGKVLAHV	Insect[1]	0.356	+3	−0.0294
Cecropin B2	RWKIFKKIEKMGRNIRDGIVKAGPAIEVLGSAKAI	Insect[2]	0.249	+6	−0.240
Dermaseptin b	DVLKKIGTVALHAGKAALGAVADTISQ	Frog[3]	0.280	+1	−0.0185
Magainin 2	GIGKFLHSAKKFGKAFVGEIMNS	Frog[4]	0.333	+4	−0.109
Melittin	GIGAVLKVLTTGLPALISWIKRKRQQ	Insect[5]	0.239	+5	−0.123
Pardaxin	GFFALIPKIISSPLFKTLLSAVGSALSSSGGQE	Fish[6]	0.0548	+1	0.0697
Maximin-4	GIGGVLLSAGKAALKGLAKVLAEKYAN	Frog[7]	0.164	+3	−0.044

[1] Bumblebee, *Megabombus pennsylvanicus*

[2] Silkworm, *Bombyx mori*

[3] Frog, *Phyllomedusa sanvagii*

[4] African clawed frog, *Xenopus laevis*

[5] Honeybee, *Apis mellifera*

[6] Red Sea Moses sole fish, *Pardachirus marmoratus*

[7] Chinese red-belly toad, *Bombina maxima*

[a] Hydrophobic moment calculated according to Eisenberg et al. (1982) with individual amino acid hydrophobicities taken from Janin (1979)

[b] Charge, not including the N- or C-termini

[c] Average hydrophobicity calculated from the individual amino acid hydrophobicities in Janin (1979)

(Budapest, Hungary). 4-Methylbenzhydrylamine (MBHA) resin was obtained from Novabiochem (Laufelfingen Switzerland). *N*,*N*′-dicyclohexylcarbodiimide (DCC), 1-hydroxybenzotriazole (HOBt), *N*,*N*′-diidopropylethylamine (DIEA), and trifluoroacetic acid (TFA) were products from Fluka (Buchs, Switzerland). Solvents (DMF, DCM, acetonitrile, diethyl-ether) for peptide synthesis and purification were purchased from Reanal (Budapest, Hungary). All other reagents were from Sigma (St. Louis, MO).

Peptide synthesis and purification

The peptides were synthesized manually by solid-phase methodology on MBHA resin (200 mg, 1.4 mmol/g) using Boc chemistry. The first amino acid, Boc-Asn-OH, and coupling reagents DCC and HOBt were used in 1.4 M excess for the resin capacity. After the coupling, the capacity of the modified resin was calculated on the basis of its N-content and was found to be 0.73 mmol/g. The Boc protecting group was removed with 33% TFA in DCM (2 + 20 min) followed by washing with DCM (5 × 0.5 min), neutralization with 10% DIEA in DCM (3 × 1 min), and DCM washing again (4 × 0.5 min). The protected amino acid derivatives and coupling reagents (DCC and HOBt) dissolved in DCM-DMF 4:1 (v/v) were used in 3 M excess for the resin capacity. The coupling reaction proceeded for 60 min at room temperature, then the resin was washed [DMF (2 × 0.5 min), DCM (3 × 0.5 min)]. The efficiency of the coupling was checked by ninhydrin assay (Kaiser et al. 1970). The amino acid side-chain protecting groups were cyclohexyl ester for Glu, benzyl for Ser, and 2-chlorobenzyloxycarbonyl for Lys. The hydroxyl group of Tyr was blocked by 2-bromobenzyloxycarbonyl group.

After assembly, the protected peptides were cleaved from the resin by 10 mL hydrogen fluoride using 0.5 g *p*-cresol as scavenger. Crude products were precipitated by dry diethyl-ether, dissolved in 10% acetic acid, and freeze-dried. The freeze-dried preparations were purified by RP-HPLC (Herbert Knauer GmbH, Berlin, Germany) using a Phenomenex Jupiter C18 column (250 × 10 mm I.D.) with 10 μm silica (300 Å pore size) (Torrance, CA) as stationary phase. The flow rate was 4 mL/min. Linear gradient elution (0 min 40% B; 5 min 40% B; 50 min 100% B) was generated using 0.1% TFA in water as eluent A and 0.1% TFA in acetonitrile/water (80:20, v/v) as eluent B. Peaks were detected at $\lambda = 220$ nm at room temperature.

Analytical HPLC was performed on a Knauer system (Herbert Knauer GmbH, Berlin, Germany) using a Phenomenex Jupiter C18 column (250 × 4.6 mm I.D., 5 μm silica, 300 Å pore size) (Torrance, CA, USA) as stationary phase. Linear gradient elution (0 min 0% B; 50 min 90% B) was generated. Flow rate of 1 mL/min was applied at ambient temperature. Peaks were detected at $\lambda = 220$ nm. The samples were dissolved in eluent B. The molecular mass value of all peptide was measured by electrospray ionization mass spectrometry (ESI–MS) performed on a Bruker Esquire 3000 plus (Germany) instrument. The samples were dissolved in acetonitrile/water (50:50, v/v) containing 0.1% acetic acid.

NMR sample preparation

For the solution NMR experiments, samples containing SDS micelles were prepared by dissolving ~2.8 mg lyophilized maximin-4 (MW = 2,612) in 700 μL 10 mM sodium-phosphate buffer (pH 5.8) containing 200 mM d_{25}-SDS and 10% D_2O. The sample pH was adjusted to 5.0 with NaOH. For the experiments in DPC micelles, a number of peptide concentrations were tested in the range of 0.4–1.5 mM while keeping the d_{38}-DPC concentration at 350 mM in the same buffer used for SDS micelles. Aqueous samples with no micelles and samples in methanol were prepared by dissolving ~5 mg peptide in *either* 700 μL buffer containing 20 mM potassium phosphate, 50 mM potassium chloride, 0.05% NaN_3, and 10% D_2O at pH 6.3, *or* 700 μL CD_3OH/H_2O (1:1, v/v) mixture.

For the solid-state NMR experiments in multilamellar vesicles (MLV), various compositions of dipalmitoylphosphatidylcholine (DPPC) and dipalmitoylphosphatidylglycerol (DPPG) were dissolved in $CHCl_3$/MeOH (2:1, v/v) to ensure thorough mixing. The solvent was removed under dry N_2 at room temperature followed by storage under vacuum overnight. Site-specifically ^{13}C- and ^{15}N-labeled maximin-4 was dissolved in buffer containing 20 mM piperazine-*N*-*N*′-bis(2-ethanesulfonic acid) (PIPES), 1 mM EDTA, pH 7.0 at room temperature. The dried lipids were resuspended in the peptide-containing buffer at 65°C to give the desired lipid/peptide molar ratio (L/P). For lyoprotection, an amount of trehalose equivalent to 20% of the dry weight of the phospholipids was also incorporated (Crowe and Crowe 1984; Rudolph and Crowe 1985). The resulting suspension was subjected to six cycles of freezing (dry ice/EtOH), warming to $T = 65°C > T_m$ (where T_m is the phase transition temperature of the phospholipids), and vortexing. The sample was lyophilized overnight and packed into a 3.2-mm outside-diameter zirconia rotor, fitted with plastic (Kel-F) end-caps and spacers.

Solution NMR spectroscopy

One- and two-dimensional solution NMR experiments were carried out on a Varian NMR System™ (600 MHz for ^1H) five-channel spectrometer using a 5-mm indirect detection triple resonance ($^1H^{13}C^{15}N$) *z*-axis gradient probe. Experiments were performed at either 40°C (SDS), 25°C (methanol) or 15°C (aqueous buffer). The ^1H resonances were assigned using a combination of two-dimensional (2D) TOCSY (Bax and Davis 1985), 2D NOESY (Kumar et al. 1980), and natural abundance ^1H-^{13}C HSQC experiments (John et al. 1992). Solvent water suppression in the former two experiments was achieved by the WATERGATE technique (Piotto et al. 1992). The TOCSY experiments implemented a decoupling in the presence of scalar interactions (DIPSI) spin lock for polarization transfer and utilized mixing times (τ_m) up to 80 ms (Shaka et al. 1988). NOESY experiments were performed at mixing times of 70, 150, 250, and 300 ms. TOCSY and NOESY spectra were acquired with a ^1H spectral width of 9,615 Hz in both dimensions. In F1 and F2, 256 and 1,024 complex data points were acquired and zero-filled to a total of 512 and 2,048 points, respectively. Gaussian and exponential weighting functions were applied in both dimensions in all spectra except for the HSQC experiments, in which the ^{13}C dimension was Gaussian weighted only. All chemical shifts were referenced to external 4,4-dimethyl-4-silapentane-1-sulfonate (DSS).

Interproton distance restraints were obtained from NOESY experiments performed with $\tau_m = 250$ ms (SDS) and $\tau_m = 300$ ms (aqueous buffer, methanol). Structure calculations were performed with ARIA (Ambiguous Restraints for Iterative Assignment, version 2.2) (Nilges et al. 1997; Linge et al. 2001; Habeck et al. 2004). Typically, in each of the seven iterations, the ten lowest-energy structures were used as templates for the next iteration, and the seven best structures were used for restraint violation analysis. The computational algorithm in the structure calculation employed torsional angle simulated annealing followed by torsional angle and then Cartesian molecular dynamics cooling stages. Structural refinement was completed in a water shell. The stereochemical quality and structural statistics of the final ensemble were determined using PROCHECK (Laskowski et al. 1993) and PROCHECK NMR (Laskowski et al. 1996).

Solid-state NMR spectroscopy

All spectra were collected on a 600-MHz Varian NMR System™ spectrometer operating with ^1H, ^{13}C, and ^{15}N frequencies of 599.72, 150.81, and 60.76 MHz, respectively, using a Varian/Chemagnetics narrow-bore 3.2-mm HXY triple resonance magic-angle spinning (MAS) probe. Rotational echo double resonance (REDOR) experiments (Gullion and Schaefer 1989a, b) on MLVs were carried out at a controlled MAS (Andrew et al. 1958; Lowe 1959) speed of 9,000 Hz. A 2.0 ms ramped cross-polarization (Hartmann and Hahn 1962) was followed by a REDOR dephasing period and then direct ^{13}C detection with a recycle delay of 3 s. A single 54-kHz ^{13}C 180° pulse was placed at the center of the REDOR dephasing time. Dephasing ^{15}N 180° pulses were applied at the middle and at the end of each rotor period and were set at 45 kHz. Experiments were performed using 80-kHz SPINAL ^1H decoupling (Sinha et al. 2005) during the dephasing and detection periods. The ^{13}C and ^{15}N transmitters were set at 175 ppm (relative to adamantane) and 105 ppm (relative to glycine), respectively. The acquisition temperature was 2°C.

Circular dichroism measurements

Circular dichroism (CD) spectra of maximin-4 in vesicle suspensions and aqueous micellar solutions were recorded with a J-815 spectropolarimeter (JASCO, Groβ-Umstadt, Germany) in quartz glass cuvettes of 1 mm optical path length (Suprasil; Hellma Optik GmbH, Jena, Germany) between 260 and 180 nm at 0.1 nm intervals. Three repeat scans at scan rate of 10 nm/min, 8 s response time, and 1 nm bandwidth were averaged for each sample. Lipid suspension samples were prepared as described for the solid-state NMR experiments, except that a 5–10 min period of ultrasonication was included after rehydration of the dried lipid film. Buffer conditions for the micellar solutions were the same as in the solution NMR experiments (10 mM sodium phosphate, pH 5.0). Samples with various lipid-to-peptide (L/P = 20, 50, 100, 200) and detergent-to-peptide (D/P = 40, 130) molar ratios were prepared and investigated. Peptide concentrations ranged between 3 and 60 μM. Lipid (~1 mM) and detergent concentrations (~10 mM) were adjusted accordingly. Spectra were baseline corrected by subtracting the spectrum of a blank sample containing all components except the peptide.

Results

Solution NMR spectroscopy

The conformation of maximin-4 was investigated in negatively charged SDS and zwitterionic DPC micelles, in aqueous buffer, and in 50% methanol. One-dimensional ^{1}H NMR spectra of the peptide in aqueous buffer (pH 6.3) show poor chemical shift dispersion (Fig. 1a), suggesting the lack of a well-defined structure. In the presence of micelles, dramatic shift changes occur in the amide proton region, demonstrating peptide folding (Fig. 1b). This is most clearly seen for residues I2, G3, V5, G10, A13, K19, and N27. In DPC, in addition to shift changes, the resonance lines become severely broadened (Fig. 1c), which unfortunately persists over a wide range of temperatures and peptide/detergent molar ratios, and prevented us from obtaining sequence-specific resonance assignments. As a compromise, in an attempt to differentiate between electrostatic and hydrophobic effects on the structure of maximin-4, along with the structure determination in SDS we also characterized the conformation of the peptide in 50% CD_3OH. The apparent similarities of the one-dimensional ^{1}H spectra in SDS and methanol in terms of both chemical shift dispersion and resonance line widths (Fig. 1b, d) suggest that the secondary structure content of the peptide in the two environments is comparable to each other.

Resonance assignment

Assignment of backbone and side-chain proton resonances of maximin-4 in the different investigated environments was accomplished using a combination of 2D TOCSY, NOESY, and natural abundance ^{13}C-HSQC experiments. In SDS micelles, resonance assignment and structure determination were performed at a detergent-to-peptide molar ratio of ~130. Upon further increasing the relative amount of SDS no further changes in chemical shifts were observed, ensuring that under these experimental conditions all of the peptide was bound. The fingerprint H_N-H_α region of the peptide obtained in SDS micelles is shown in Fig. 2a. The assignment was complicated by resonance overlap and an inefficient relay of magnetization in the TOCSY experiment. Due to the latter, some of the residues did not display a complete spin system (i.e., H_β, H_γ resonances of leucines, lysines were missing), complicating the distinction between different types of amino acids. To overcome this problem, 2D NOESY spectra acquired with increasing mixing times were analyzed. In addition to assessing the H_N-$H_{aliphatic}$ correlations, the assignment was aided by the H_N-H_N region of the NOESY spectra (Fig. 2b), in which most of the sequential $d_{NN}(i, i + 1)$, as well as a few $d_{NN}(i, i + 2)$ correlations were detected throughout the peptide backbone. The corresponding H_N-H_α and H_N-H_N spectral regions of maximin-4 obtained in aqueous buffer in the absence of micelles are shown for comparison in panels C and D of Fig. 2. The full sequence-specific assignments of maximin-4 in the different environments are given in the Supplementary Information (Tables S1–S3).

NMR structural parameters

In aqueous buffer, the H_α chemical shifts of maximin-4 indicate a slight preference for an α-helical conformation, in particular toward the C-terminal region of the peptide chain (Fig. 3a). In spite of this, long-range distance restraints are missing from the NOESY spectra, suggesting the lack of sufficient intramolecular contacts to form a stable secondary structure. The presence of SDS induces changes in H_α chemical shifts throughout the entire sequence. These shift changes are consistent with a more pronounced α-helical content and are in agreement with the CD spectroscopic studies (see below). Similar H_α secondary shifts were detected in 50% methanol with perhaps more characteristic deviations from random coil values for residues V5–A9 and somewhat reduced effects for residues K11–L17.

Secondary chemical shifts were also determined for the backbone amide protons. These parameters are known to be related to the location of amino acid residues in

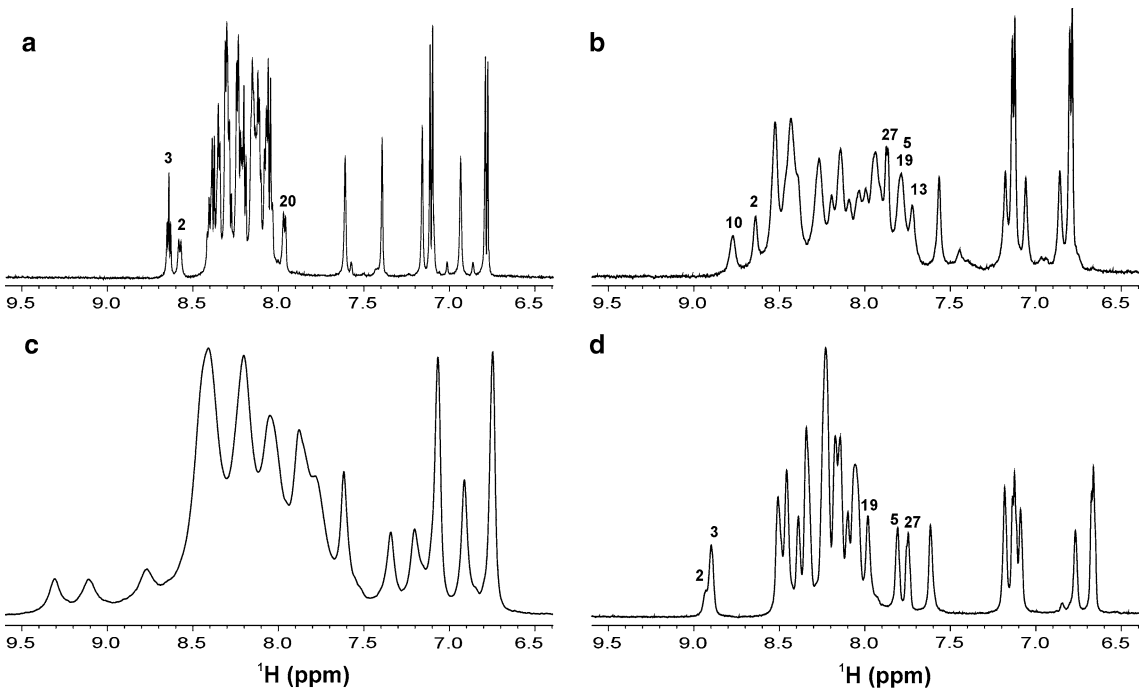

Fig. 1 Aromatic and amide proton regions of one-dimensional ^{1}H spectra of maximin-4 (1.5 mM) in **a** 20 mM potassium phosphate, 50 mM potassium chloride, 0.05% NaN_3 at pH 6.3 and 15°C, **b** 200 mM d_{25}-SDS, 10 mM sodium phosphate at pH 5 and 40°C, **c** 350 mM d_{38}-DPC and same conditions as in (**b**), and **d** CD_3OH/H_2O (1:1, v/v) at 25°C. Resonances for which chemical shift changes are most easily seen are labeled with the corresponding residue number

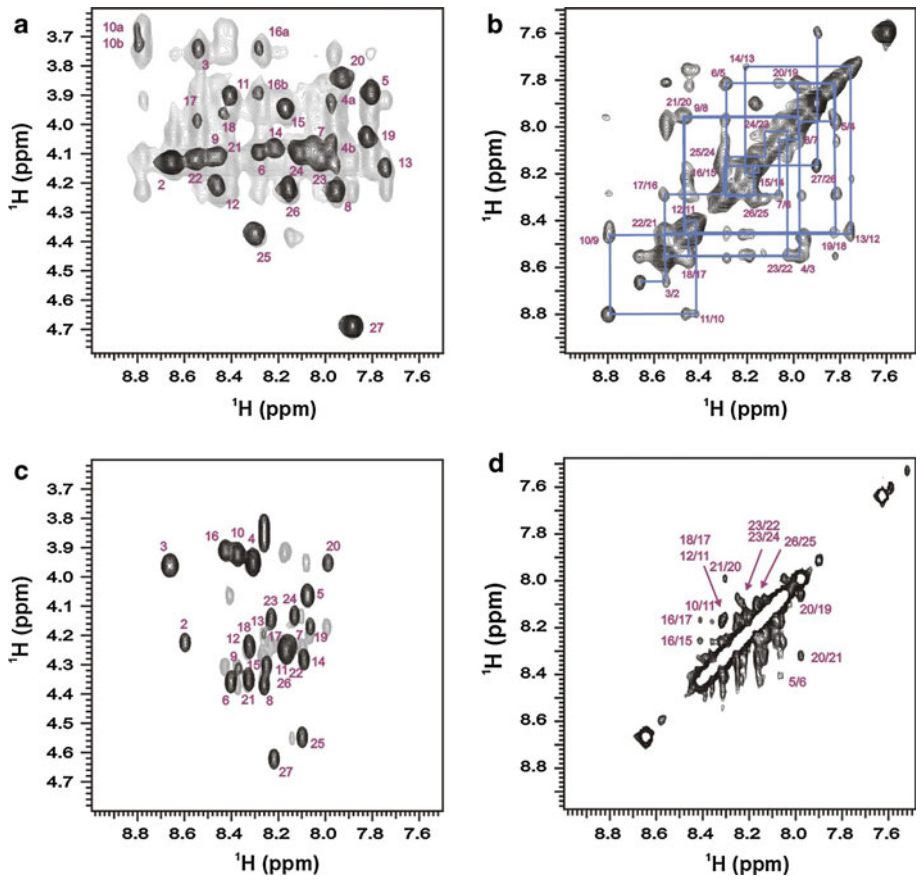

Fig. 2 Regions of two-dimensional ^{1}H-^{1}H spectra of maximin-4 (1.5 mM) in aqueous buffer in the presence (**a**, **b**) and absence (**c**, **d**) of SDS micelles showing the intra- and interresidue correlations used to help establish sequence-specific resonance assignments. **a** Superimposed H_α-H_N region of 2D TOCSY (*black*) and 2D NOESY (*grey*) spectra and **b** the H_N-H_N region of 2D NOESY spectrum in 200 mM d_{25}-SDS (pH 5, 40°C). **c**, **d** The same spectral regions for the peptide in pure aqueous buffer (pH 6.3, 15°C). Cross-peaks are labeled according to their assignment. The path over the sequential HN_i-HN_{i+1} connectivities for the NOESY spectrum (250 ms) collected in SDS is shown as a *continuous line*

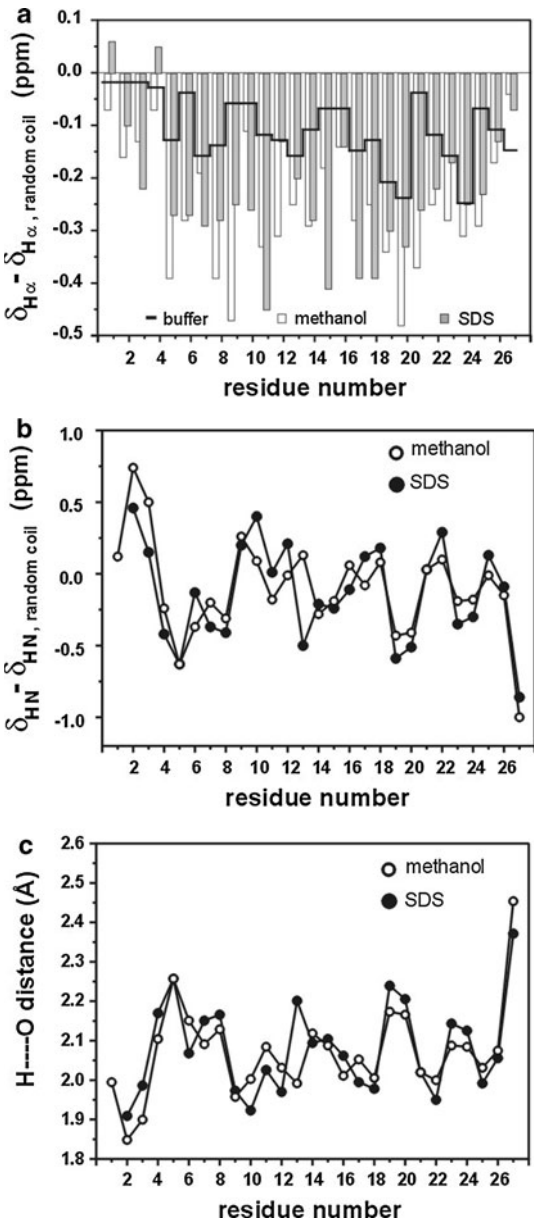

Fig. 3 Summary of NMR secondary shifts. **a** Deviations of H_α chemical shifts from random coil values for maximin-4 in 50% methanol (*white columns*), in 200 mM SDS (*grey columns*), and in aqueous buffer (*continuous black line*). **b** Deviations of H_N chemical shifts from random coil values for maximin-4 in 200 mM SDS (*filled circles*) and in 50% methanol (*open circles*). **c** Hydrogen-bond lengths (the distance from the carbonyl oxygen to the amide proton) obtained from the amide proton chemical shifts in SDS (*filled circles*) and in methanol (*open circles*). Random coil chemical shifts were taken from Wüthrich (1986). Hydrogen-bond lengths were calculated according to the equation $\Delta\delta_{HN} = 19.2d^{-3} - 2.3$, where $\Delta\delta_{HN}$ is the difference between the detected and random coil amide proton chemical shift in ppm and d is the NH···O distance in Å (Wagner et al. 1983)

amphipathic α-helices and have been associated with H-bond lengths (Zhou et al. 1992). Differences between the observed H_N chemical shifts and those expected in a random coil are shown in Fig. 3b as a function of the amino acid position in micelles and in methanol. Hydrogen-bond distances were calculated from the observed $\Delta\delta_{HN}$ values according to the formula by Wagner et al. (1983) and are shown in Fig. 3c. The curves display the expected periodicity (Kuntz et al. 1991), in particular for the C-terminal half of the peptide chain with maximum positive $\Delta\delta_{HN}$ values at positions A18, L21, and Y25, and maximum negative numbers at K19 and E23. The values obtained in micelles and in methanol show a remarkable similarity, indicating that the location of polar and apolar residues *within* the helices are similar in the two environments. The largest difference occurs in the middle of the chain, at A13, where a significantly longer NH–OC distance is indicated in SDS. Smaller differences are observed for a stretch of three consecutive residues starting at G10, indicating shorter H-bonds in micelles for these amino acid positions. It is also noticeable that, in the C-terminal half of the chain, maxima and minima are somewhat more pronounced in SDS (e.g., positions K19, A22, and E23) and that the periodicity of the curves breaks around G16 in both environments. In the N-terminal half, periodicity still seems to exist, but with a less tight appearance compared with the repeat pattern of 3–4. We note that, as chemical shifts of H_N protons are extremely sensitive to environmental conditions, we carried out our analysis using two different random coil references (Wüthrich 1986; Merutka et al. 1995). The periodicity of the curves and the position of minima and maxima seemed to be insensitive to which reference was used.

In addition to chemical shifts, typical ^{1}H-^{1}H NOE correlations are indicative measures of peptide secondary structure (Wüthrich 1986). While in aqueous buffer the detected NOESY cross-peaks were mostly limited to intraresidue and sequential $(i, i + 1)$ ^{1}H-^{1}H correlations, for the micelle-bound peptide and for maximin-4 in 50% CD_3OH, several $d_{\alpha N}(i, i + 2)$, $d_{\alpha N}(i, i + 3)$, $d_{\alpha\beta}(i, i + 3)$, and $d_{\alpha\beta}(i, i + 4)$ NOE correlations characteristic of α-helical conformation were observed (Fig. 4a, b). The $(i, i + 3)$ and $(i, i + 4)$ spatial proximities as well as other long-range NOEs were particularly prevalent in the C-terminal half of the peptide chain in both environments. The difference in backbone orientation of maximin-4 in SDS and methanol, indicated by the H_α and H_N secondary chemical shifts in the middle of the chain, was corroborated by the NOE connectivities in this region. The side-chain contacts of K15 and K19 with K11, observed for the peptide in methanol, were replaced with A13–L17 and A13–A18 contacts in SDS. Unambiguous nonsequential NOEs observed at and near the kink region are listed in Table 2 for both environments. In addition, tables listing all the nonsequential NOEs in SDS and in methanol are presented in the Supplementary Material (Tables S4–S5).

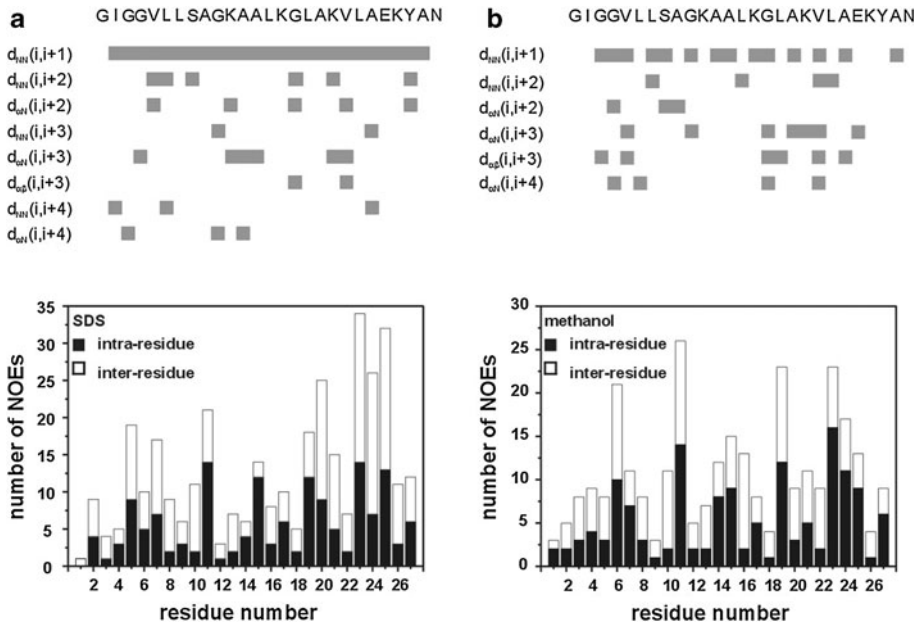

Fig. 4 Diagnostic interatomic distance restraints and histograms showing the number of intra- and interresidue NOEs as a function of residue number obtained for maximin-4 in **a** SDS (pH 5, 40°C) and **b** 50% methanol (25°C)

A more stable C-terminal half of the peptide is also suggested by H/D exchange experiments. Upon ~16 h exposure to D_2O of the micelle-bound peptide, a number of residues in the C-terminal half (L14, G16, L17, A18, A22, E23, and K24) remained protected from the solvent, whereas in the N-terminal half only residues L6 and L7 showed detectable H_α-H_N correlations in 2D NOESY spectra ($\tau_{mix} = 70$ ms). In a similar experiment in methanol, solvent-protected residues were exclusively in the C-terminal half and restricted to the region A18–E23. No sign of correlation was observed between protected amide proton resonances and calculated intrinsic exchange rates (Bai et al. 1993), suggesting that the protection we observed arises from the secondary and tertiary structure of the peptide; for instance, in spite of having one of the highest calculated intrinsic exchange rates, G16 (located near the kink) was one of the nine residues whose amide proton remained protected in SDS after prolonged exposure to D_2O.

Calculated liquid-state NMR structure of maximin-4

The results of structure calculations are summarized in Fig. 5 and Table 3. Independent calculations gave the 15 lowest-energy structures with a high degree of convergence in both environments. Representative structures of the ensembles were determined by calculating the mean coordinates using a subroutine of ARIA. According to this, a highly disordered N-terminal region is followed by a helical segment, a break, and another helix, both in SDS and in methanol. In methanol, helix I (L6–A12) appears to be a 3_{10}-helix and is substantially shorter than the C-terminal α-helix (K15–A26), whereas in SDS the two α-helices have approximately the same length (V5–A13, L17–K24). In both environments, the N-terminal half of helix I is less ordered, whereas its C-terminal half, the kink region, and helix II (residues G10–Y25 all together) are well defined with an average RMSD from the mean of 0.28 ± 0.18 Å in SDS and 0.52 ± 0.12 Å in methanol for their backbone heavy atoms. Side-chains in the same region give an overall average RMSD from the mean of 0.90 ± 0.48 Å (SDS) and 1.23 ± 0.36 Å (methanol).

The peptide in SDS adopts a tight V shape with an interhelical angle of approximately 70° (Fig. 5c). Favorable contacts between the C-terminal end of helix I and the N-terminal part of helix II are the main source of stabilization for the kink. This is achieved by the contacts of A12, located near the C-terminal end of helix I. Its carbonyl oxygen is within H-bonding distance of the NH of residues G16 and L17 with favorable N–H–O angles to both. The kink is further stabilized by a hydrophobic cluster formed by the side-chain moieties of A12, A13, and L17. In methanol, the hinge between the two helices appears to be less tight with an interhelical angle of 90° (Fig. 5d), and is stabilized merely by van der Waals interactions.

Although the overall topology of the structures obtained in SDS and in methanol are similar, differences in the geometry of the kink result in different relative orientations of the two helices, which in turn has a major consequence for the arrangement of the positively charged lysine side-chains (Fig. 5e, f). While in SDS they are all located on the outer, convex face of the structure, extending away from the peptide backbone, in methanol two among the four lysines and the negatively charged glutamate side-chain lie on the inner, concave face of the molecule. Electrostatic

Table 2 List of unambiguous nonsequential upper distance limits at and near the kink region (Gly_{10}–Lys_{19}) used for the structure determination of maximin-4 in SDS micelles and in 50% CD_3OH. Full lists of nonsequential NOEs are provided in the Supplementary Material (Tables S4–S5)

Residue 1	Atom 1	Residue 2	Atom 2	Constraint (Å)
SDS				
GLY 10	HA3	LEU 14	HN	4.23
GLY 10	HN	ALA 13	HN	5.98
GLY 10	HA3	ALA 13	HN	4.50
GLY 10	HA3	LEU 14	HD21	4.15
LYS 11	HG3	LEU 14	HN	4.91
LYS 11	HA	ALA 13	HN	4.87
ALA 12	HA	LYS 15	HN	3.92
ALA 12	HA	GLY 16	HN	4.26
ALA 13	HN	LYS 15	HD2	5.07
ALA 13	HA	GLY 16	HN	3.90
GLY 16	HA3	LYS 19	HB2	4.77
GLY 16	HA3	ALA 18	HN	4.65
GLY 16	HN	ALA 18	HN	5.12
CD_3OH				
GLY 10	HA2	ALA 13	HN	5.05
LYS 11	HG3	GLY 16	HA3	3.69
LYS 11	HG3	LYS 19	HN	4.12
LYS 11	HE2	LYS 19	HD2	5.14
LYS 11	HE2	LYS 19	HN	4.20
LYS 11	HG3	LYS 19	HD2	2.69
ALA 13	HN	LYS 15	HG3	5.95
LEU 14	HN	GLY 16	HN	3.98
GLY 16	HA3	LYS 19	HN	4.81
GLY 16	HA2	LYS 19	HD2	3.80
GLY 16	HA2	LYS 19	HN	4.52
GLY 16	HA3	LYS 19	HD2	4.38
GLY 16	HA2	LYS 19	HB2	5.19

potential maps of the contact surface of the mean structure of maximin-4 in SDS and methanol were computed using the program MOLMOL (Koradi et al. 1996) and are shown in Fig. 6. The charge distribution in SDS shows a hydrophobic core flanked by positively charged regions on each side. Intriguingly, the two charged regions (one in the N- and one in the C-terminal half of the peptide) are located on the opposite faces of the two helices, providing the peptide with more opportunities to engage in electrostatic interactions. The carboxylate group of E23 is located on the convex face right in the middle of the ammonium groups of K19 and K24, at ~5 Å from each. In the presence of methanol, the charge distribution is strikingly different. With only K15 and K24 located on the convex face, the other remaining charged regions seem to sequester themselves in the space between the two helices. Here, the carboxylate of E23 and the ammonium group of K19 come into close proximity to each other (~3 Å) and likely form a salt bridge, providing further stabilization for helix II.

Conformation of maximin-4 in lipid bilayers

As a lipid bilayer is considered to be a better approximation for mimicking a cell membrane than detergent micelles are, the backbone conformation of maximin-4 was investigated in phospholipid bilayers using CD spectroscopy and solid-state NMR. Our first aim is to establish that the overall structure of maximin-4 formed upon binding to SDS micelles is similar to the conformation when bound to lipid bilayers. The CD spectra of maximin-4 in SDS micelles (detergent-to-peptide molar ratio of ~130) and DMPC/DMPG (1:1, v/v) vesicles (lipid-to-peptide molar ratio of 50) are shown in Fig. 7. In both environments, the spectra are typical for α-helical conformations as reflected by the negative ellipticity at ~208–210 and ~219–222 nm. Titration experiments of peptide solutions with detergent and lipid suspensions showed that the peptides are in a completely bound state at the relative concentrations shown. The helical content of the peptide was calculated to be 82% in SDS and 85% in DMPC/DMPG (1:1, v/v). These data suggest that the overall conformation of maximin-4 in negatively charged lipid bilayers must resemble the structure we obtained in SDS micelles.

To obtain site-specific information, in particular regarding the N-terminal helix of maximin-4, we turned to solid-state NMR. To determine site-specific ^{13}C chemical shifts characteristic of peptide secondary structure, we embedded maximin-4 in MLVs of various phospholipid compositions and used REDOR, a magic-angle spinning technique (thus maintaining high-resolution) which detects weak heteronuclear dipolar couplings (Gullion and Schaefer 1989a, b). To this aim we introduced clusters of ^{13}C and ^{15}N labels at three distinct positions along the peptide sequence, allowing us to probe the secondary structure at positions L6, A13, and L21. The diminished intensity of the resonance lines at 177.1 and 16.3 ppm in Fig. 8 is a manifestation of the dipolar coupling between the proximate ^{13}C and ^{15}N isotope labels in [**1-^{13}C**]Leu_6-[^{15}N]Leu_7-[**3-^{13}C**]Ala_{13}-[^{15}N]Leu_{14}-maximin-4-NH_2 and unambiguously identifies the resonance frequency of the carbonyl carbon of L6 and the methyl carbon of A13. The observed chemical shifts are consistent with an α-helical conformation (Kricheldorf and Müller 1983; Saito 1986) at both amino acid positions of the membrane-embedded peptide. The chemical shift of the carbonyl carbon of L21 was determined in a similar dipolar recoupling experiment on a different sample and was found to be 177.3 ppm, thus confirming the α-helical secondary structure at all three positions in DPPC/DPPG (2:1, v/v) bilayers. The peptide

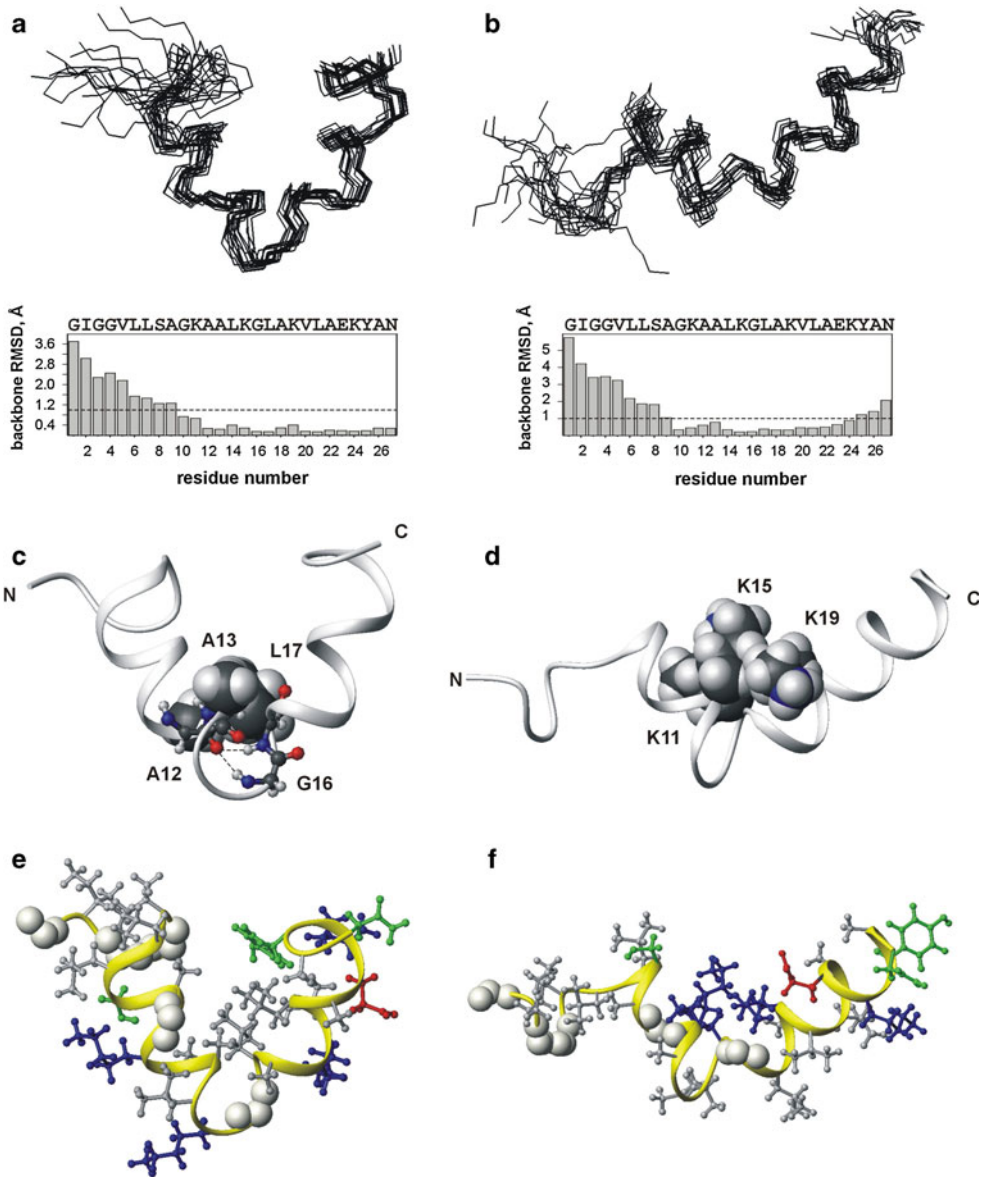

Fig. 5 Results of NMR structure calculation. **a**, **b** *Top* Superpositions of the 15 lowest-energy conformations obtained for the backbone atoms of maximin-4 (1.5 mM) in SDS (200 mM) (**a**), and in 50% methanol (**b**). *Bottom* Average backbone RMSDs from the mean of the 15 lowest-energy conformations of maximin-4 in SDS and in 50% methanol. **c**, **d** Ribbon diagram of the mean structure of maximin-4 in SDS (**c**), and in 50% methanol (**d**). Stabilization of the kinked region in SDS arises from hydrogen bonds (A12–G16 and A12–L17), and from a hydrophobic cluster formed by the side-chains of A12, A13, and L17. van der Waals interactions between the side-chains of K11, K15, and K19 seem to be the main source of stabilization in methanol. **e**, **f** The same ribbon diagrams as in (**c**) and (**d**) showing the amino acid side-chains. Color coding: hydrophobic residues in *grey*, lysines in *blue*, glutamate in *red*, other polar residues in *green*. Heavy atoms of glycines are represented as *spheres*

was also investigated in DPPC/DPPG (1:1, v/v) and in pure DPPC bilayers. No chemical shift changes within experimental error occurred for the investigated amino acid positions, and they all remained consistent with the helical conformation irrespective of the molar ratio of negatively charged DPPG.

The α-helical conformation of maximin-4 in both negatively charged and zwitterionic membranes is also supported by our oriented CD spectroscopic data presented in the accompanying paper (Heinzmann et al. 2010). As the peptide shows no hemolytic activity at its antimicrobial concentration, our findings indicate that helicity in itself is not sufficient for maximin-4 to induce lysis. Rather, as has been suggested by studies of other AMPs and model peptides (Dathe et al. 1996; Oren et al. 2002), the lytic activity is influenced by more subtle combination of electrostatic and hydrophobic effects such as segregation between positively charged and hydrophobic residues within the polypeptide chain.

Discussion

The majority of antimicrobial peptides such as maximin-4 are known to exert their action through direct, non-receptor-mediated interaction with the bacterial cell membrane, resulting in pore formation and dissipation of the electrochemical gradient across the lipid bilayer (Shai 1999; Epand and Vogel 1999; Boman 2003). In some cases there are indications that the killing mechanism may involve a more robust disintegration of the pathogenic cell membrane (Wu et al. 1999; Mangoni et al. 2004). Membrane

Table 3 Statistics of the NMR structure and stereochemical quality of maximin-4 in SDS micelles (40°C, pH 5) and H_2O/CD_3OH (1:1, v/v) (25°C)

	SDS	CD_3OH
NOEs		
Intraresidue	151	144
Interresidue, sequential	108	75
Interresidue, nonsequential	92	84
Ensemble RMSD values		
Average main-chain RMSD from mean coordinates, Å		
Helix I (L5–A13 in SDS, L6–A12 in CD_3OH)	1.06 ± 0.64	0.82 ± 0.28
Kink (L14–G16 in SDS, A13–L14 in CD_3OH)	0.27 ± 0.13	0.56 ± 0.07
Helix II (L17–K24 in SDS, K15–A26 in CD_3OH)	0.21 ± 0.09	0.55 ± 0.22
Statistics		
Ramachandran plot statistics		
Residues in most favored regions [A, B, L], % (#)	66.7 (14)	81.0 (17)
Residues in additionally allowed regions [a, b, l, p], % (#)	33.3 (7)	19.0 (4)
Residues in generously allowed regions [∼a, ∼b, ∼l, ∼p], % (#)	0.0 (0)	0.0 (0)
Residues in disallowed regions, % (#)	0.0 (0)	0.0 (0)
Main-chain statistics		
SD of ω angle, degrees	7.0	4.1
Bad contacts/100 residues	N/A	N/A
C_α chirality, SD of ζ angle, degrees	1.6	0.5
H-bond energy, kcal/mole	0.7	0.9
Overall *G*-factor	−0.5	0.1
Side-chain statistics		
χ-1 *gauche* minus SD, degrees	16.4	37.3
χ-1 *trans* SD, degrees	28.9	16.1
χ-1 *gauche* plus SD, degrees	24.9	16.3
χ-1 pooled SD, degrees	26.1	22.7
χ-2 *trans* SD, degrees	10.1	19.2

All statistics were carried out using PROCHECK. The two end-residues and the glycines were excluded from the Ramachandran analysis

permeabilization is supposed to occur in two stages. First, the electrostatic interactions between phospholipid headgroups and the positively charged amino acid side-chains play a key role in binding the peptides to the membrane surface. Subsequently, immersion of the peptide into the hydrophobic core of the bilayer induces lysis. To understand the subtle interplay of electrostatic, hydrophobic, and restructuring effects leading to pore formation, an atomic-level picture of the peptide–membrane interaction is necessary.

In the current study we have determined the liquid-state NMR structure of maximin-4, a 27-residue AMP, in two different membrane-mimetic environments (SDS micelles and 50% methanol), and we obtained site-specific chemical shifts characteristic of peptide secondary structure in lipid bilayers using solid-state NMR. According to the liquid-state NMR data, the peptide adopts a helix–break–helix conformation both in negatively charged micelles and in the presence of methanol. The predominantly α-helical character is in good agreement with the CD data obtained for maximin-4 in lipid vesicles. Moreover, the chemical shifts obtained by solid-state NMR confirm the position of the helices, suggesting that the structure in micelles and bilayers should closely resemble each other.

Similar kinked arrangements have been found for a number of AMPs and have often been associated with their ability to induce lysis (Chi et al. 2007; Oh et al. 2000; Pukala et al. 2004; Xiao et al. 2009). In most of the reported cases, the hinge region occurs around a glycine or a proline residue, and the increased flexibility allows the peptide to find the most appropriate orientation to insert into the bilayer, while at the same time maintaining contacts with the lipid headgroups. The amino acid sequence of maximin-4 is such that, in case of a single rigid α-helix, charged and other polar residues would be distributed around the entire helical cross-section. The break in the helix dissects the sequence into two separate structural units, each in itself possessing a more pronounced segregation of polar and apolar residues. Enhanced amphipathicity increases the affinity of the peptide for the bilayer, whereas the hinge between the two segments allows them to take different orientations. As AMPs have been found to cause a thinning in the bilayer (Ludtke et al. 1995; Lee et al. 2004), the segment of maximin-4 staying in contact

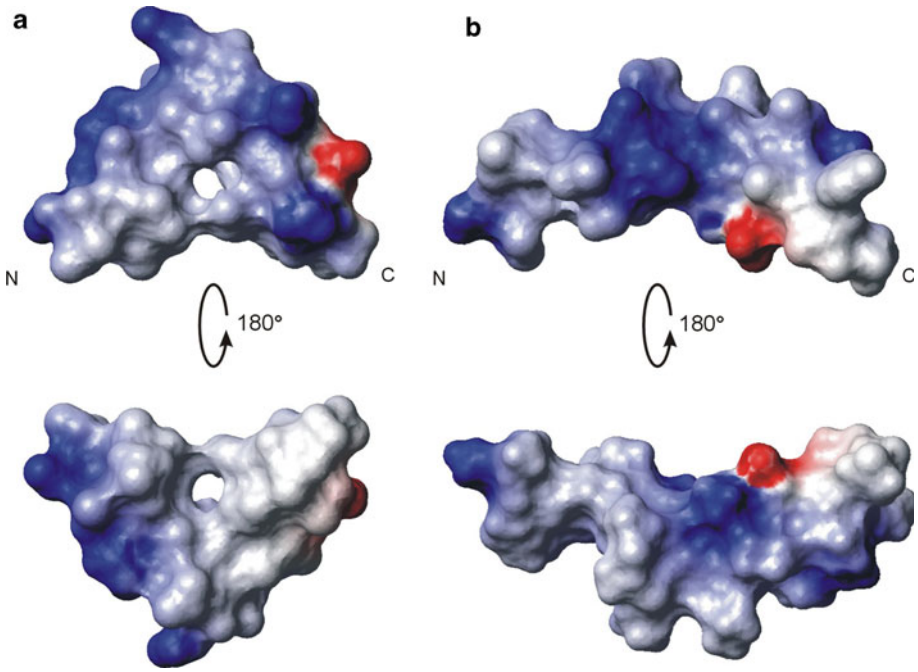

Fig. 6 Charge distribution on the surface of maximin-4 shown for the mean structure in **a** SDS, and **b** in 50% methanol. Positive and negative potentials are colored in *blue* and *red*, respectively

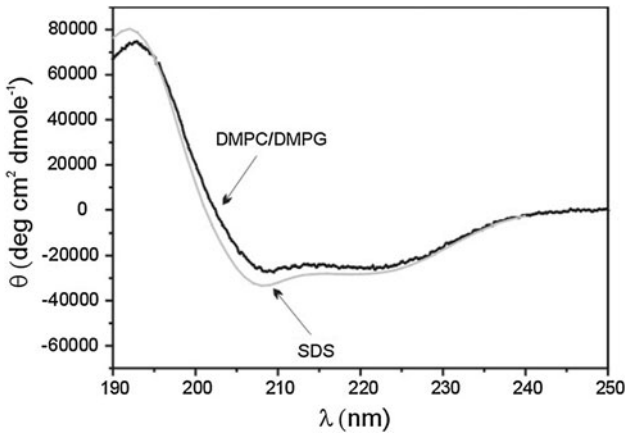

Fig. 7 Circular dichroism spectra of maximin-4 in unilamellar lipid vesicles [10 μM peptide, 1 mM DMPC:DMPG (1:1, v/v)] and detergent micelles (70 μM maximin-4, 9.1 mM SDS)

with the lipid headgroups is likely not perpendicular to the membrane normal, but rather has a tilted orientation. Although it remains to be determined whether maximin-4 acts alone or similarly to many other AMPs forms an assembly in the bilayer, the flexible hinge also enables the segments inserted into the hydrophobic membrane core to associate by their hydrophobic faces. This would lead to a "funnel-like" arrangement in which helices staying in contact with the headgroups form the downhill upper part of the funnel, the inserted helices form the stem, and the kinks are at the bottleneck. Similar funnel-like pores are common among ion channels, and have also been proposed for AMPs, specifically for pardaxin (Porcelli et al. 2004) and gaegurin 4 (Chi et al. 2007), in the past.

Another important structural feature of maximin-4 that we observed both in SDS and in methanol is its disordered N-terminal region. A similarly disordered N-terminal segment has been found in LL-37, a cathelicidin-derived human AMP, with an overall topology reminiscent of the conformation of maximin-4 (Porcelli et al. 2008). Although the exact functional role of the disordered N-terminal segment has not been elucidated yet, it has been shown to be essential for the antimicrobial action of LL-37 (Ciornei et al. 2005).

Even though the overall topology of maximin-4 (i.e., position of the kink, length of the helices) is similar in SDS and in methanol, the atomic details of these two structures are markedly different. Major differences are observed in terms of the forces stabilizing the kink region as well as in the shape and charge distribution of the molecules. In SDS, backbone and side-chain interactions in the middle of the chain (A12–L17) give rise to a V-shaped structure with overall dimensions of 27 Å × 23 Å × 15 Å possessing large positively charged patches on both legs of the V. In methanol, the stabilizing interactions in the hinge region appear to be less tight, resulting in a more elongated molecular shape with dimensions of 35 Å × 19 Å × 14 Å and positively charged regions that are more restricted in space.

Although, due to its isotropic nature, methanol is only a crude membrane mimetic, the differences between the conformations adopted by maximin-4 in SDS and methanol may have implications for the bacterial selectivity of the peptide. The main source of the selectivity of AMPs is thought to arise from differences in the lipid composition

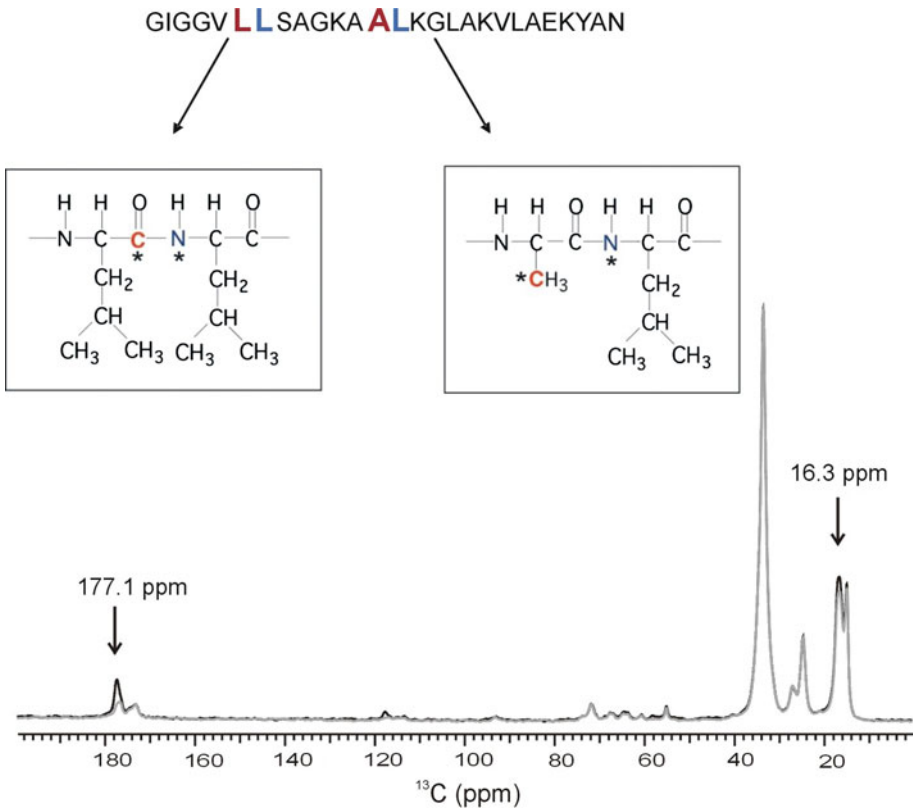

Fig. 8 150.8-MHz ^{13}C full-echo (*black*) and ^{15}N-dephased (*grey*) REDOR spectra of [**1-^{13}C**]Leu_6-[^{15}N]Leu_7-[**3-^{13}C**]Ala_{13}-[^{15}N]Leu_{14}-maximin-4-NH_2 incorporated into multilamellar vesicles of DPPC and DPPG (2:1) at lipid-to-peptide molar ratio of 20, after 48 rotor cycles of dipolar evolution with MAS at 9,000 Hz. The position of ^{13}C and ^{15}N labels exploited in spectral editing is shown at the top of the figure. Peptide signals arising from [1-^{13}C]Leu_6 and [3-^{13}C]Ala_{13} were selected by their dipolar couplings to proximate ^{15}N spins ([^{15}N]Leu_7 and [^{15}N]Leu_{14}, respectively). Diminished signal intensities (*grey*) at 177.1 and 16.3 ppm report an α-helical conformation at residues Leu_6 and Ala_{13} of the peptide chain. The position of the ^{13}C signal arising from [1-^{13}C]Leu_6 was also confirmed by a 16-T_r $^{13}C\{^{15}N\}$ REDOR experiment

of eukaryotic and prokaryotic cell membranes. While the outer leaflet of eukaryotic membranes is composed of zwitterionic phospholipids (Verkleij et al. 1973), bacterial cell membranes contain a high proportion of negatively charged phospholipids in both the outer and the inner leaflets of the lipid bilayer (Ratledge 1998). The long, amphipathic lysine side-chains extending from the peptide backbone in diverse orientations allow the peptide chains to penetrate deeply into the hydrophobic core of the micelle, while at the same time engaging themselves in electrostatic interactions with the negatively charged SDS headgroups (Segrest et al. 1990). It is likely that these electrostatic peptide–micelle interactions provide further stabilization of the kinked maximin-4 in SDS. A similar dual effect (high affinity combined with deep insertion) may be responsible for the strong activity of the peptide in negatively charged lipid bilayers such as the prokaryotic cell membrane. Unlike in prokaryotic systems, the driving force of pore formation in eukaryotic membranes is dominated by the hydrophobic effect. The shallow, elongated structure of maximin-4 in methanol suggests that, in the absence of favorable charge–charge interactions, the peptide may not have the ability to penetrate deeply enough into the hydrophobic lipid core to cause substantial leakage.

The distribution of lysine side-chains on the convex versus concave faces of the molecule also has a profound effect on the size of the relative polar/nonpolar face of the helices, a key determinant of the curvature strain that is imposed on lipid bilayers by the peptide chains (Tytler et al. 1993; Epand et al. 1995). The effect of the polar angle on the lytic activity of AMPs has been studied extensively and seems to have different influences on peptide binding and their permeabilization efficiency. In an investigation of magainin analogues (Wieprecht et al. 1997), peptide binding was found to increase with increasing polar angle and negatively charged phospholipid content, whereas the permeabilization efficiency was largest for small polar angles and low negative membrane charges. As a result, a decrease in the polar face of the peptide was found to lead to enhanced dye release from negatively charged phospholipid vesicles, but reduced the lytic activity against vesicles with high zwitterionic phospholipid content.

The relative size of the hydrophilic versus hydrophobic face of peptides has also been associated with their orientation in lipid bilayers. According to the classification by Brasseur (1991), peptides with small hydrophilic angle and high overall hydrophobicity tend to form transmembrane pores, whereas peptides with approximately equivalent hydrophilic and hydrophobic angles orient themselves parallel to the membrane surface. In both SDS and methanol, different polar angles are inferred for helix I and II of maximin-4. In both environments, helix I has a small

hydrophilic face (45°), whereas the cross-section of helix II appears to be more polar (180° in SDS, 270° in methanol). Based on these observations in membrane mimetics, it seems plausible that, if hypothesizing a funnel-like arrangement in lipid bilayers, helix II might be the one which is responsible for keeping intimate contacts with the headgroup region, whereas the more dynamic N-terminal half inserts into the hydrophobic core of the membrane.

In conclusion, we have determined the three-dimensional structure of maximin-4 in negatively charged SDS micelles, and independently in 50% methanol. In both environments, following a disordered N-terminal segment, the peptide chain adopts a helix–break–helix conformation, suggesting that the kinked nature is an intrinsic property of the peptide. Despite the similar topology, major differences occurred in the interactions stabilizing the kink region and the shape and charge distribution of the molecule. Thus, maximin-4 is an AMP with the capability of assuming at least two distinct well-defined conformations, depending on the physicochemical properties of the environment, with both conformations reflecting its apparently intrinsic desire to be bent. The structural differences we found in SDS and methanol might imply different mechanisms of action of maximin-4 towards negatively charged and neutral membranes, and might explain in part the selectivity of the peptide. As a first step in obtaining a detailed picture of the membrane interactions of maximin-4, our studies also contribute to a better understanding of the mode of action of AMPs in general. Further liquid-state and solid-state NMR experiments in the accompanying paper (Heinzmann et al. 2010) are aimed at determining the molecular alignment of maximin-4 lipid bilayers, to shed further light on the mechanism of pore formation.

Acknowledgments The authors thank Dr. Gábor Mező for helpful discussions on peptide synthesis. O.T. thanks Dr. Stephan Grage (Karlsruhe Institute of Technology) for helpful discussions on the manuscript. Z.B. is grateful for the support of the Bolyai János Fellowship program of the Hungarian Academy of Sciences. This work was supported by grants from the Hungarian Research Fund (OTKA) F68326 and the Hungarian GVOP-3.2.1.-2004-04-0210/3.0 project.

References

Andres E, Dimarcq JL (2005) Clinical development of antimicrobial peptides. Int J Antimicrob Agents 25:448–452

Andreu D, Rivas L (1998) Animal antimicrobial peptides: an overview. Biopolymers 47:415–433

Andrew ER, Bradbury A, Eades RG (1958) Nuclear magnetic resonance spectra from a crystal rotated at high speed. Nature 182:1659

Bai Y, Milne JS, Mayne L, Englander SW (1993) Primary structure effects on peptide group hydrogen exchange. Proteins 17:75–86

Bax A, Davis DG (1985) MLEV-17 based two-dimensional homonuclear magnetization transfer spectroscopy. J Magn Reson 65:355–360

Boman HG (2003) Antibacterial peptides: basic facts and emerging concepts. J Intern Med 254:197–215

Brasseur R (1991) Differentiation of lipid-associating helices by use of three-dimensional molecular hydrophobicity potential calculations. J Biol Chem 266:16120–16127

Chi SW, Kim JS, Kim DH, Lee SH, Park YH, Han KH (2007) Solution structure and membrane interaction mode of an antimicrobial peptide gaegurin 4. Biochem Biophys Res Commun 352:592–597

Ciornei CD, Sigurdardóttir T, Schmidtchen A, Bodelsson M (2005) Antimicrobial and chemoattractant activity, lipopolysaccharide neutralization, cytotoxicity, and inhibition by serum of analogs of human cathelicidin LL-37. Antimicrob Agents Chemother 49:2845–2850

Crowe JH, Crowe LM (1984) Preservation of membranes in anhydrobiotic organisms: the role of trehalose. Science 223:701–704

da Silva A Jr, Teschke O (2003) Effects of the antimicrobial peptide PGLa on live Escherichia coli. Biochim Biophys Acta 1643: 95–103

Dathe M, Wieprecht T (1999) Structural features of helical antimicrobial peptides: their potential to modulate activity on model membranes and biological cells. Biochim Biophys Acta 1462: 71–87

Dathe M, Schümann M, Wieprecht T, Winkler A, Beyermann M, Krause E, Matsuzaki K, Murase O, Bienert M (1996) Peptide helicity and membrane surface charge modulate the balance of electrostatic and hydrophobic interactions with lipid bilayers and biological membranes. Biochemistry 35:12612–12622

Drawz SM, Bonomo RA (2010) Three decades of beta-lactamase inhibitors. Clin Microbiol Rev 23:160–201

Eisenberg D, Weiss RM, Terwilliger TC (1982) The helical hydrophobic moment: a measure of the amphiphilicity of a helix. Nature 299:371–374

English BK, Gaur AH (2010) The use and abuse of antibiotics and the development of antibiotic resistance. Adv Exp Med Biol 659:73–82

Epand RM, Vogel HJ (1999) Diversity of antimicrobial peptides and their mechanisms of action. Biochim Biophys Acta 1462:11–28

Epand RM, Shai Y, Segrest JP, Anantharamaiah GM (1995) Mechanisms for the modulation of membrane bilayer properties by amphipathic helical peptides. Biopolymers 37:319–338

Ge M, Chen Z, Onishi HR, Kohler J, Silver LL, Kerns R, Fukuzawa S, Thompson C, Kahne D (1999) Vancomycin derivatives that inhibit peptidoglycan biosynthesis without binding D-Ala-D-Ala. Science 284:507–511

Gibson BW, Tang D, Mandrell R, Kelly M, Spindel ER (1991) Bombinin-like peptides with antimicrobial activity from skin secretions of the Asian toad, Bombina orientalis. J Biol Chem 266:23103–23111

Gullion T, Schaefer J (1989a) Rotational echo double-resonance NMR. J Magn Reson 81:196–200

Gullion T, Schaefer J (1989b) Detection of weak heteronuclear dipolar coupling by rotational echo double-resonance. Adv Magn Res 13:57–83

Habeck M, Rieping W, Linge JP, Nilges M (2004) NOE assignment with ARIA 2.0. Methods Mol Biol 278. In: Downing AK (ed) Protein NMR techniques. Humana Press, Inc., Totowa

Hancock REW (1997) Peptide antibiotics. Lancet 349:418–422

Hancock REW, Diamond G (2000) The role of cationic antimicrobial peptides in innate host defenses. Trends Microbiol 8:402–410

Harris F, Dennison SR, Phoenix DA (2009) Anionic antimicrobial peptides from eukaryotic organisms. Curr Protein Pept Sci 10:585–606

Hartmann SR, Hahn EL (1962) Nuclear double resonance in the rotating frame. Phys Rev 128:2042–2053

Heinzmann R, Grage SL, Schalck C, Bürck J, Bánóczi Z, Toke O, Ulrich AS (2010) A kinked antimicrobial peptide from *Bombina maxima*. II. Behavior in phospholipid bilayers. doi:s00249-011-0668-x

Janin J (1979) Surface and inside volumes in globular proteins. Nature 277:491–492

John BK, Plant D, Webb P, Hurd RE (1992) Effective combination of gradients and crafted RF pulses for water suppression in biological samples. J Magn Reson 95:200–206

Kaatz GW (2005) Bacterial efflux pump inhibition. Curr Opin Investig Drugs 6:191–198

Kaiser E, Colescott RL, Bossinger CD, Cook PI (1970) Color test of detection of free amino groups in the solid phase synthesis of peptides. Anal Biochem 34:595–598

Koradi R, Billeter M, Küthrich K (1996) MOLMOL: a program for display and analysis of macromolecular structures. J Mol Graph 14:51–55

Kricheldorf HR, Müller D (1983) Secondary structure of peptides. 3. Carbon-13 NMR cross polarization/magic angle spinning spectroscopy characterization of solid polypeptides. Macromolecules 16:615–623

Kumar A, Ernst RR, Wüthrich K (1980) A two-dimensional nuclear Overhauser enhancement (2D NOESY) experiment for the elucidation of complete proton-proton cross relaxation networks in biological macromolecules. Biochem Biophys Res Commun 95:1–6

Kuntz ID, Kosen PA, Craig EC (1991) Amide chemical shifts in many helices in peptides and proteins are periodic. J Am Chem Soc 113:1406–1408

Lai R, Liu H, Hui Lee W, Zhang Y (2002a) An anionic antimicrobial peptide from toad Bombina maxima. Biochem Biophys Res Commun 295:796–799

Lai R, Zheng YT, Shen JH, Liu GJ, Liu H, Lee WH, Tang SZ, Zhang Y (2002b) Antimicrobial peptides from skin secretions of Chinese red belly toad Bombina maxima. Peptides 23:427–435

Laskowski RA, MacArthur MW, Moss DS, Thornton JM (1993) *PROCHECK*: a program to check the stereochemical quality of protein structures. J Appl Chrystallogr 26:283–291

Laskowski RA, Rullmann JA, MacArthur MW, Kaptein R, Thornton JM (1996) AQUA and PROCHECK-NMR: programs for checking the quality of protein structures solved by NMR. J Biomol NMR 8:477–486

Lee MT, Chen FY, Huang HW (2004) Energetics of pore formation induced by membrane active peptides. Biochemistry 43:3590–3599

Lin H, Walsh CT (2004) A chemoenzymatic approach to glycopeptide antibiotics. J Am Chem Soc 126:13998–14003

Linge JP, O'Donoghue SI, Nilges M (2001) Automated assignment of ambiguous nuclear overhauser effects with ARIA. Methods Enzymol 339:71–90

Lowe IJ (1959) Free induction decays of rotating solids. Phys Rev Lett 2:285–287

Ludtke SJ, He K, Huang HW (1995) Membrane thinning caused by magainin. Biochemistry 34:16764–16769

Mangoni ML, Papo N, Barra D, Simmaco M, Bozzi A, Di Giulio A, Rinaldi AC (2004) Effects of the antimicrobial peptide temporin L on cell morphology, membrane permeability and viability of Escherichia coli. Biochem J 380:859–865

Matsuzaki K (1999) Why and how are peptide-lipid intereactions utilized for self-defense? Magainins and tachyplesins as archetypes. Biochim Biophys Acta 1462:1–10

Merutka G, Dyson HJ, Wright PE (1995) 'Random-coil' ^{1}H chemical shifts obtained as a function of temperature and trifluoroethanol concentration for peptide series GGXGG. J Biomol NMR 5:14–24

Nicolas P, Mor A (1995) Peptides as weapons against microorganisms in the chemical defense system of vertebrates. Ann Rev Microbiol 49:277–304

Nilges M, Macias MJ, O'Donoghue SI, Oschkinat HJ (1997) Automated NOESY interpretation with ambiguous distance restraints: the refined NMR solution structure of the pleckstrin homology domain from beta-spectrin. Mol Biol 269:408–422

Oh D, Shin SY, Lee S, Kang JH, Kim SD, Ryu PD, Hahm KS, Kim Y (2000) Role of the hinge region and the tryptophan residue in the synthetic antimicrobial peptides, cecropin A(1-8)-magainin 2(1-12) and its analogues, on their antibiotic activities and structures. Biochemistry 39:11855–11864

Oren Z, Ramesh J, Avrahami D, Suryaprakash N, Shai Y, Jelinek R (2002) Structures and mode of membrane interaction of a short α helical lytic peptide and its diastereomer determined by NMR, FTIR, and fluorescence spectroscopy. Eur J Biochem 269:3869–3880

Park CB, Kim HS, Kim SC (1998) Mechanism of action of the antimicrobial peptide buforin II: buforin II kills microorganisms by penetrating the cell membrane and inhibiting cellular functions. Biochem Biophys Res Comm 244:253–257

Piotto M, Saudek V, Sklenar V (1992) Gradient-tailored excitation for single-quantum NMR spectroscopy of aqueous solutions. J Biomol NMR 2:661–665

Porcelli F, Buck B, Lee D-K, Hallock KJ, Ramamoorthy A, Veglia G (2004) Structure and orientation of pardaxin determined by NMR experiments in model membranes. J Biol Chem 279: 45815–45823

Porcelli F, Verardi R, Shi L, Henzler-Wildman KA, Ramamoorthy A, Veglia G (2008) NMR structure of the cathelicidin-derived human antimicrobial peptide LL-37 in dodecylphosphocholine micelles. Biochemistry 47:5565–5572

Pukala TL, Brinkworth CS, Carver JA, Bowie JH (2004) Investigating the importance of the flexible hinge in caerin 1.1: solution structures and activity of two synthetically modified caerin peptides. Biochemistry 43:937–944

Ratledge C, Wilkinson SG (eds) (1998) Microbial Lipids, vol 1. Academic, London

Rudolph AS, Crowe JJ (1985) Membrane stabilization during freezing: the role of two natural cryoprotectants, trehalose and proline. Cryobiology 22:367–377

Saito H (1986) Conformation-dependent ^{13}C chemical shifts: a new means of conformational characterization as obtained by high-resolution solid-state ^{13}C NMR. Magn Res Chem 24:835–852

Segrest JP, de Loof H, Dohlman JG, Brouillettem CG, Anantharamaiah GM (1990) Amphipathic helix motif: classes and properties. Proteins 8:103–117

Shai Y (1999) Mechanisms of the binding, insertion and destabilization of phospholipid bilayer membranes by α-helical antimicrobial and cell non-selective membrane-lytic peptides. Biochim Biophys Acta 1462:55–70

Shai Y (2002) Mode of action of membrane active antimicrobial peptides. Biopolymers 66:236–248

Shaka AJ, Lee CJ, Pines A (1988) Iterative schemes for bilinear operators: application to spin decoupling. J Magn Reson 77:274–293

Sieber SA, Marahiel MA (2005) Molecular mechanisms underlying nonribosomal peptide synthesis: approaches to new antibiotics. Chem Rev 105:715–738

Simmaco M, Barra D, Chiarini F, Noviello L, Melchiorri P, Kreil G, Richter K (1991) A family of bombinin-related peptides from the skin of Bombina variegate. Eur J Biochem 199:217–222

Sinha N, Grant CV, Wu CH, De Angelis AA, Howell SC, Opella SJ (2005) SPINAL modulated decoupling in high field double- and triple-resonance solid-state NMR experiments on stationary samples. J Magn Reson 177:197–202

Toke O (2005) Antimicrobial peptides: new candidates in the fight against bacterial infections. Biopolymers 80:717–735

Tossi A, Sandri L, Giangaspero A (2000) Amphipathic, alpha-helical antimicrobial peptides. Biopolymers 55:4–30

Tytler EM, Segrest JP, Epand EM, Nie SQ, Epand RF, Mishra VK, Venkatachalapathi YV, Anantharamaiah GM (1993) Reciprocal effects of apolipoprotein and lytic peptide analogs on membranes. Cross-sectional molecular shapes of amphipathic alpha helixes control membrane stability. J Biol Chem 268:22112–22118

Ulvatne H, Samuelsen O, Haukland HH, Kramer M, Vorland LH (2004) Lactoferricin B inhibits bacterial macromolecular synthesis in Escherichia coli and Bacillus subtilis. FEMS Microbiol Lett 237:377–384

Van't Hof W, Veerman ECI, Helmerhorst EJ, Amerongenm AVN (2001) Antimicrobial peptides: properties and applicability. Biol Chem 382:597–619

Verkleij AJ, Zwaal FA, Roelofsen B, Comfurius P, Kastelijn D, van Deenen LL (1973) The asymmetric distribution of phospholipids in the human red cell membrane. A combined study using phospholipases and freeze-etch electron microscopy. Biochim Biophys Acta 323:178–193

Wagner G, Pardi A, Wüthrich K (1983) Hydrogen bond length and 1H NMR chemical shifts in proteins. J Am Chem Soc 105: 5948–5949

Walsh CT (2000) Molecular mechanisms that confer antibacterial drug resistance. Nature 406:775–781

Wieprecht T, Dathe M, Epand RM, Beyermann M, Krause E, Maloy WL, MacDonald DL, Bienert M (1997) Influence of the angle subtended by the positively charged helix face on the membrane activity of amphipathic, antibacterial peptides. Biochemistry 36:12869–12880

Wu M, Maier E, Benz R, Hancock REW (1999) Mechanism of interaction of different classes of cationic antimicrobial peptides with planar bilayers and with the cytoplasmic membrane of Escherichia coli. Biochemistry 38:7235–7242

Wüthrich K (1986) NMR of proteins and nucleic acids. Wiley, New York

Xiao Y, Herrera AI, Bommineni YR, Soulages JL, Prakash O, Zhang G (2009) The central kink region of fowlicidin-2, an α-helical host defense peptide, is critically involved in bacterial killing and endotoxin neutralization. J Innate Immun 1:268–280

Zhou NE, Zhou B-Y, Sykes BD, Hodges RS (1992) Relationship between amide proton chemical shifts and hydrogen bonding in amphipathic α-helical peptides. J Am Chem Soc 114:4320–4326